

Effect of Al doping on the magnetic properties of $\text{Sr}_{0.1}\text{Ca}_{0.6}\text{La}_{0.3}\text{Al}_x\text{Fe}_{12-x}\text{O}_{19}$ hexaferrite magnets

Yujie Yang*, Juxiang Shao, Fanhou Wang and Duohui Huang

Computational Physics Key Laboratory of Sichuan Province, School of Physics and Electronic Engineering, Yibin University, Yibin 644007, P. R. China

Al substituted M-type hexaferrite samples, $\text{Sr}_{0.1}\text{Ca}_{0.6}\text{La}_{0.3}\text{Al}_x\text{Fe}_{12-x}\text{O}_{19}$ ($0 \leq x \leq 1.4$), were synthesized by the ceramic process. The X-ray diffraction (XRD) was used to examine the phase composition of the magnetic powders. The XRD patterns of the magnetic powders at Al content (x) ≤ 0.8 show the M-type strontium hexaferrite phase with $\alpha\text{-Fe}_2\text{O}_3$ as a second phase. At Al content (x) ≥ 1.0 , there are single magnetoplumbite phase patterns. The images of the M-type hexaferrite magnets were observed by a field emission scanning electron microscopy (FE-SEM). The grain particles of the magnets are hexagonal platelet-like shape, and the grain size decreases with the increase of Al concentration (x). A permanent magnetic measuring system was used to measure the magnetic properties of the magnets. The remanence (B_r) decreases with Al content (x) from 0 to 1.4. The intrinsic coercivity (H_{ci}) increases with Al content (x) from 0 to 1.4. While the magnetic induction coercivity (H_{cb}) first increases with Al content (x) from 0 to 0.6 and then decreases at Al content (x) ≥ 0.6 .

Key words: X-ray diffraction, Magnetic properties, Al doping, M-type hexaferrites.

Introduction

M-type hexaferrites have a wide span of applications in various fields such as magnetic recording, microwave devices, telecommunications and permanent magnets [1]. These hexaferrites are available at low cost and possess large magnetocrystalline anisotropy, moderate energy product, high Curie temperature, excellent chemical stability, high corrosion and electrical resistivity [2].

In order to utilize these materials in a number of applications, many studies have been done to improve the magnetic properties of M-type hexaferrites. Partial substitutions of Sr^{2+} or Ba^{2+} ions by La^{3+} , Pr^{3+} , Nd^{3+} and Gd^{3+} ions, and of Fe^{3+} ions by Cu^{2+} , Zn^{2+} , Co^{2+} , Ga^{3+} , Cr^{3+} , Mn^{3+} and Al^{3+} ions have been studied [3–15]. Li et al. have synthesized the Nd-doped strontium ferrites $\text{SrNd}_x\text{Fe}_{12-x}\text{O}_{19}$ ($x = 1.0$) have reported that for the La-substituted strontium hexaferrite $\text{SrLa}_x\text{Fe}_{12-x}\text{O}_{19}$ ($x = 0\text{--}1.0$) film, at $x = 0.2$, the sample exhibits maximum coercivity (H_c) (5986 Oe) [3]. Bhat et al. have synthesized the Nd-substituted strontium hexaferrites $\text{Sr}_{1-x}\text{Nd}_x\text{Fe}_{12}\text{O}_{19}$ ($x = 0\text{--}0.20$) [5]. Vizhi et al. have prepared the cobalt substituted barium strontium hexaferrite $\text{Ba}_{0.5}\text{Sr}_{0.5}\text{Fe}_{12-x}\text{Co}_x\text{O}_{19}$ ($x = 0, 0.5, 0.7$ and 0.9) by one-step citrate gel combustion method followed by annealing and found that the maximum saturation magnetization (M_s) was obtained for

the $x = 0.5$ cobalt substitution [9]. Sharma et al. have synthesized Mn-substituted doped barium hexaferrites by high energy ball milling and found that Mn ions occupy all iron sites, and decrease the magnetization and increase the coercivity [13]. Wang et al. have reported the improvement of the coercivity of strontium induced by substitution of Al^{3+} ions for Fe^{3+} ions [11]. In addition, M-type hexaferrites with combined substitution such as La-Co, La-Zn, La-Cu, Pr-Ni, Tb-Zn, etc. have been investigated [16–20]. Yang et al. have synthesized the La-Co substituted Sr-Ca hexaferrites by the solid state reaction method and found that with increasing La-Co contents the remanence continuously increased, and the coercivity first increased and then decreased [16].

Ca is the same group of the periodic table, and the same electronic configuration as that of Sr and Ba. There are few previous reports about M-type hexaferrites with calcium substitution [21–23]. Chen et al. have prepared M-type $\text{Sr}_{0.61-x}\text{La}_{0.39}\text{Ca}_x\text{Fe}_{11.7}\text{Co}_{0.3}\text{O}_{19}$ ($x = 0, 0.1, 0.2, 0.3$) by microwave calcining and found that the coercivity and saturation magnetization at $x = 0.2$ reach the maximum values, respectively [21]. Thus, in the present study, Al^{3+} ions are used to dope the Fe^{3+} in order to tailor the magnetic properties of M-type SrCaLa hexaferrites.

In this work, the $\text{Sr}_{0.1}\text{Ca}_{0.6}\text{La}_{0.3}\text{Al}_x\text{Fe}_{12-x}\text{O}_{19}$ hexaferrite magnets have been synthesized by the ceramic process. And the influence of Al substitution on the magnetic properties of $\text{Sr}_{0.1}\text{Ca}_{0.6}\text{La}_{0.3}\text{Al}_x\text{Fe}_{12-x}\text{O}_{19}$ hexaferrite magnets is investigated.

*Corresponding author:
Tel : +86-831-3531171
Fax: +86-831-3531161
E-mail: loyaltty-yyj@163.com

Experimental Procedure

The ceramic process was used to synthesize the M-type hexaferrite samples. In the present work, the commercial powders of CaCO_3 (99 wt%), SrCO_3 (99wt%), La_2O_3 (99 wt%), Al_2O_3 (99 wt%) and Fe_2O_3 (99 wt%) were used as the raw materials. Powders of the starting materials were accurately weighed according to the nominal formula of $\text{Sr}_{0.1}\text{Ca}_{0.6}\text{La}_{0.3}\text{Al}_x\text{Fe}_{12-x}\text{O}_{19}$, where the Al concentration (x) varies from 0.0 to 1.4 with about 0.2 increment. In the first stage, mixed powders of the precursor materials prepared by the wet-mixing method were calcined in a box furnace at 1260 °C for 2 hrs in the air. The calcined samples were shattered to particles less than 100 μm using a vibration mill, and then wet-milled with suitable additives (CaCO_3 , SrCO_3 , SiO_2 and Cr_2O_3) for 16 hrs in a ball-mill. The finely milled slurry was compacted into disc-shaped pellets (30 mm diameter, about 15 mm thickness) under 310 MPa in the magnetic field of 800 kA/m, which was parallel to the pressing direction. In the second stage, the pressed pellets were sintered in a box furnace at 1185 °C for 1.5 hrs in the air.

The phase components of the presintered magnetic powders were characterized by a PANalytical X'Pert Pro diffractometer in continuous mode with $\text{Cu K}\alpha$ radiation. Morphologies of the sintered magnets were observed by a Hitachi S-4800 field emission scanning electron microscopy (FE-SEM). Magnetic properties of the sintered magnets were measured at room temperature by a permanent magnetic measuring system (NIM-2000HF, made by the National Institute of Metrology of China).

Results and Discussion

Fig. 1 shows the XRD patterns of the M-type hexaferrite $\text{Sr}_{0.1}\text{Ca}_{0.6}\text{La}_{0.3}\text{Al}_x\text{Fe}_{12-x}\text{O}_{19}$ magnetic powders with Al concentration (x) varies from 0.0 to 1.4. As seen from Fig. 1, for the magnetic powder with $x \leq 0.8$, the XRD patterns show the M-type strontium hexaferrite phase, and also exhibit $\alpha\text{-Fe}_2\text{O}_3$ as a second phase. When Al concentration (x) ≥ 1.0 , there are single magnetoplumbite phase patterns. The $\alpha\text{-Fe}_2\text{O}_3$ phase for the magnetic powders with x from 0 to 0.8 could be due to the incomplete reaction under the synthesis conditions.

The lattice parameters c and a of the M-type hexaferrite $\text{Sr}_{0.1}\text{Ca}_{0.6}\text{La}_{0.3}\text{Al}_x\text{Fe}_{12-x}\text{O}_{19}$ magnetic powders with Al concentration (x) from 0.0 to 1.4 are calculated from the XRD data by the following formula [24]:

$$\frac{1}{d_{hkl}^2} = \frac{4}{3} \times \frac{h^2 + hk + k^2}{a^2} + \frac{l^2}{c^2} \quad (1)$$

where d_{hkl} is the inter-planer spacing value, and h , k and l are the Miller indices. The unit cell volume (V_{cell}) is calculated by the following equation [11]:

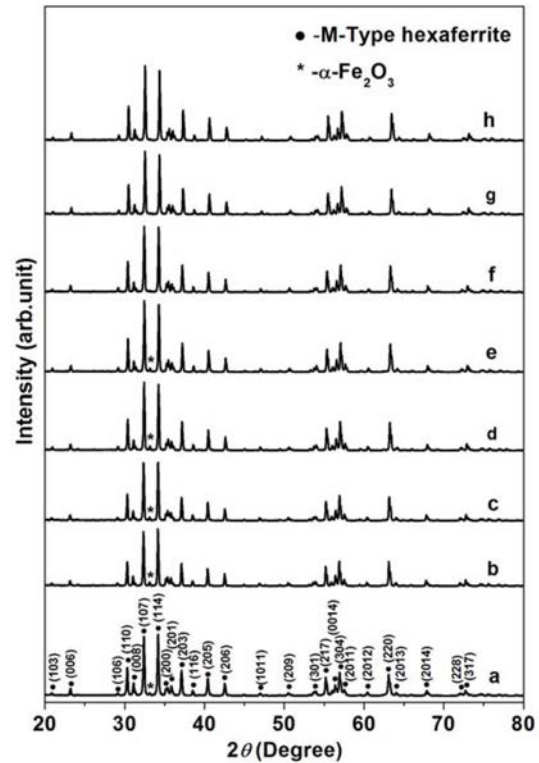


Fig. 1. The XRD patterns of the Al substituted M-type hexaferrite $\text{Sr}_{0.1}\text{Ca}_{0.6}\text{La}_{0.3}\text{Al}_x\text{Fe}_{12-x}\text{O}_{19}$ magnetic powders.

Table 1. Lattice parameters c and a , ratio of c/a , crystallite size (D) and cell volume (V_{cell}) for the hexaferrite $\text{Sr}_{0.1}\text{Ca}_{0.6}\text{La}_{0.3}\text{Al}_x\text{Fe}_{12-x}\text{O}_{19}$ magnetic powders with different Al concentration (x).

Al concentration (x)	c (Å)	a (Å)	c/a	D (nm)	V (Å ³)
0.0	23.027	5.892	3.908	43.29	692.3
0.2	23.020	5.891	3.908	53.09	691.8
0.4	22.984	5.888	3.904	51.75	690.0
0.6	22.982	5.880	3.909	51.91	688.1
0.8	22.963	5.879	3.906	51.28	687.3
1.0	22.956	5.872	3.909	49.72	685.5
1.2	22.897	5.861	3.907	51.28	681.1
1.4	22.879	5.859	3.905	51.76	680.1

$$V_{cell} = \frac{\sqrt{3}}{2} a^2 c \quad (2)$$

The crystallite size of M-type hexaferrites samples is calculated by the following relation [11]:

$$D = \frac{K\lambda}{\beta \cos \theta} \quad (3)$$

where the value of shape factor K is 0.89, λ is the X-ray wavelength, β is the full width of diffraction lines at half-width of maximum intensity and θ is the peak position. The values of lattice parameters c and a , c/a ratios, crystallite size (D) and unit cell volume (V_{cell}) are shown in Table 1. It is clear that with as Al concentration (x) is increased from 0.0 to 1.4, the

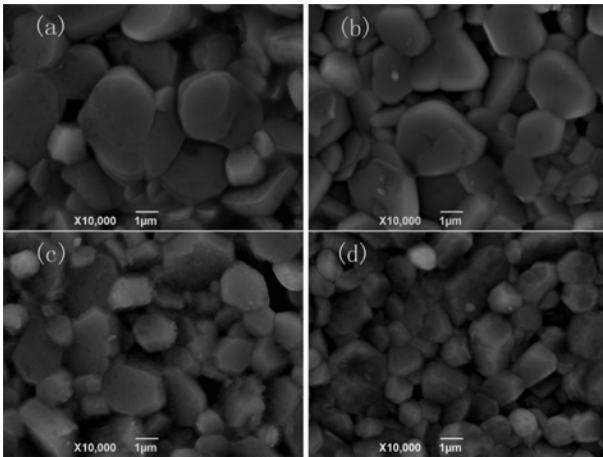


Fig. 2. Representative FE-SEM images of the M-type hexaferrite $\text{Sr}_{0.1}\text{Ca}_{0.6}\text{La}_{0.3}\text{Al}_x\text{Fe}_{12-x}\text{O}_{19}$ magnets for samples: (a) $x = 0.0$, (b) $x = 0.6$, (c) $x = 1.0$ and (d) $x = 1.4$.

lattice parameters c and a of the M-type hexaferrite $\text{Sr}_{0.1}\text{Ca}_{0.6}\text{La}_{0.3}\text{Al}_x\text{Fe}_{12-x}\text{O}_{19}$ magnetic powders decrease. This can be attributed to the fact that the ionic radii of Al^{3+} ions (0.535 \AA) are smaller than that of Fe^{3+} ions (0.645 \AA). As shown in Table 1, the c/a ratios of the magnetic powers Al concentration (x) from 0.0 to 1.4 remains almost unchanged.

The typical FE-SEM images of the M-type hexaferrite $\text{Sr}_{0.1}\text{Ca}_{0.6}\text{La}_{0.3}\text{Al}_x\text{Fe}_{12-x}\text{O}_{19}$ magnets with Al concentration (x) of 0, 0.6, 1.0 and 1.4 are shown in Fig. 2. As seen from the FE-SEM images, grain particles of the magnets are hexagonal platelet-like shape, and the particle size decreases with increasing Al concentration (x). This indicates that Al^{3+} ions could inhibit the particle growth of M-type hexaferrites. The average particle size of the magnets as shown in Fig. 2 is larger than the critical size of 650 nm [25] for the single domain magnetic particle. This shows that all magnets are multi-domain structures.

Fig. 3 shows the representative demagnetizing curves of the M-type hexaferrite $\text{Sr}_{0.1}\text{Ca}_{0.6}\text{La}_{0.3}\text{Al}_x\text{Fe}_{12-x}\text{O}_{19}$ magnets with Al concentration (x) of 0, 0.6, 1.0 and 1.4. The remanence (B_r), the intrinsic coercivity (H_{ci}), magnetic induction coercivity (H_{cb}) and maximum energy product $[(BH)_{\max}]$ are derived from the demagnetizing curves. Fig. 6 shows the variation of remanence (B_r) as a function of Al concentration (x) for the M-type hexaferrite $\text{Sr}_{0.1}\text{Ca}_{0.6}\text{La}_{0.3}\text{Al}_x\text{Fe}_{12-x}\text{O}_{19}$ magnets. It can be seen from Fig. 6 that the value of B_r for the magnets decreases with Al concentration (x) from 379.2 mT at $x = 0$ to 242.4 mT at $x = 1.4$. In the M-type hexaferrite, the Fe^{3+} ions occupy five different interstitial sites, i.e. tetrahedral $4f_1$ (downward spin), bipyramidal 2b (upward spin), and three octahedral sites 12k (upward spin), $4f_2$ (downward spin), and 2a (upward spin). For the M-type hexaferrite, the magnetic moments of Fe^{3+} ions are arranged collinearly because of the existence of super-exchange interaction.

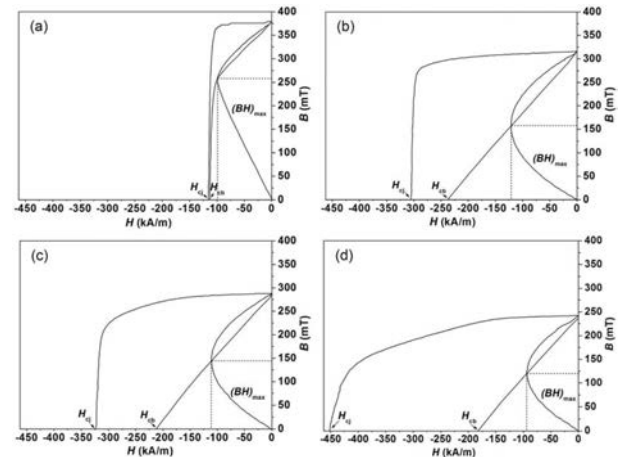


Fig. 3. Representative demagnetizing curves of the M-type hexaferrite $\text{Sr}_{0.1}\text{Ca}_{0.6}\text{La}_{0.3}\text{Al}_x\text{Fe}_{12-x}\text{O}_{19}$ magnets with Al concentration (x) of: (a) $x = 0.0$, (b) $x = 0.6$, (c) $x = 1.0$ and (d) $x = 1.4$.

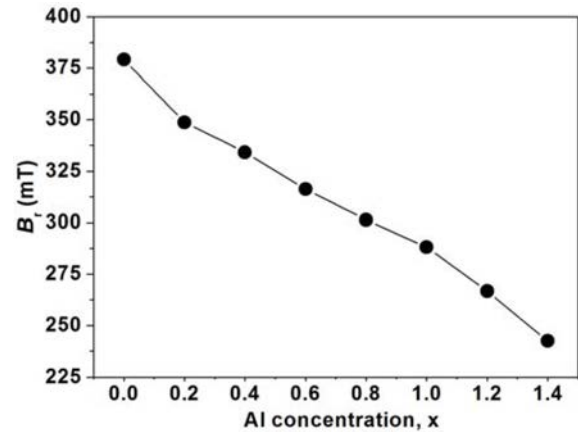


Fig. 4. The remanence (B_r) as a function of Al concentration (x) for the M-type hexaferrite $\text{Sr}_{0.1}\text{Ca}_{0.6}\text{La}_{0.3}\text{Al}_x\text{Fe}_{12-x}\text{O}_{19}$ magnets.

The results of Mössbauer spectra exhibited that Al^{3+} ions have a strong preference for the 2a, 12k, $4f_1$ and $4f_2$ sites [26, 27]. Therefore, the decrease of B_r for the magnets with Al concentration (x) from 0 to 1.4 should be due to the following two factors. On the one hand, Al^{3+} ($0 \mu_B$) ions substitute Fe^{3+} ($5 \mu_B$) ions in the M-type hexaferrite. This will cause the magnetic moment of the M-type hexaferrite to decrease, and thus cause the value of B_r to decrease. On the other hand, the super-exchange interaction between metallic ions in the M-type hexaferrite is weakened because of the non-magnetic Al^{3+} ions substituting magnetic Fe^{3+} ions, which leads to the decrease of B_r for the magnets.

The variations of the intrinsic coercivity (H_{ci}) and magnetic induction coercivity (H_{cb}) as a function of Al concentration (x) for the M-type hexaferrite $\text{Sr}_{0.1}\text{Ca}_{0.6}\text{La}_{0.3}\text{Al}_x\text{Fe}_{12-x}\text{O}_{19}$ magnets are shown in Fig. 5. It is seen that the value of H_{ci} for the magnets increases with Al concentration (x) from 0.0 to 1.4, while the value of H_{cb} for the magnets first increases with Al concentration (x) from 0.0 to 0.6, and then decreases with Al

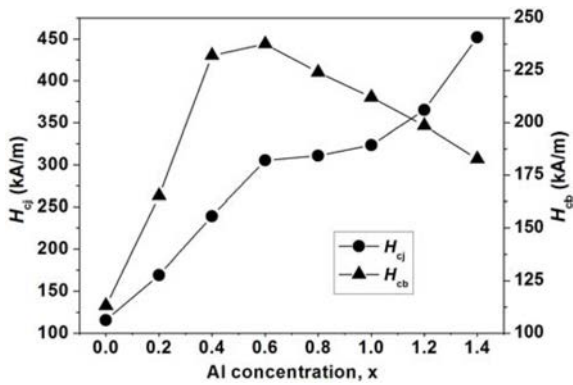


Fig. 5. The intrinsic coercivity (H_{cj}) and magnetic induction coercivity (H_{cb}) as a function of Al concentration (x) for the M-type hexaferrite $\text{Sr}_{0.1}\text{Ca}_{0.6}\text{La}_{0.3}\text{Al}_x\text{Fe}_{12-x}\text{O}_{19}$ magnets.

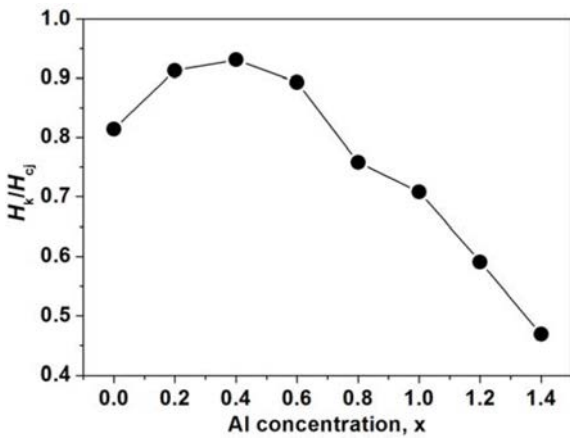


Fig. 6. H_k/H_{cj} ratios as a function of Al concentration (x) for the M-type hexaferrite $\text{Sr}_{0.1}\text{Ca}_{0.6}\text{La}_{0.3}\text{Al}_x\text{Fe}_{12-x}\text{O}_{19}$ magnets.

concentration (x) from 0.6 to 1.4. It is known that the coercivity is inversely proportional to M_s theoretically and can be described by the below equation [28]:

$$H_c = \alpha \times \frac{2K}{M_s} \quad (4)$$

where α is the orientation factor, K is the magnetocrystalline anisotropy constant and M_s is the saturation magnetization. Therefore, according to the formula (4), the increase of H_{cj} is mainly due to the decrease of remanence (B_r) with Al concentration (x) from 0.0 to 1.4. The particle size decreases with increasing Al concentration (x) also results in the increase of H_{cj} with Al concentration (x). The effect of Al concentration (x) on the H_k/H_{cj} ratio of the M-type hexaferrite $\text{Sr}_{0.1}\text{Ca}_{0.6}\text{La}_{0.3}\text{Al}_x\text{Fe}_{12-x}\text{O}_{19}$ magnets is shown in Fig. 6. The H_k/H_{cj} ratio is one of the important indicators of the magnetic properties for the permanent magnets, and can intuitively indicate the rectangularity of the demagnetizing curves for the magnets. The H_k/H_{cj} ratio characterizes the stability of the magnets under dynamic working conditions [29]. It can be seen from Fig. 6 that the ratio H_k/H_{cj} ratio first increases with Al concentration (x) from 0.0 to 0.4, and then decreases when Al concentration (x) is above 0.4.

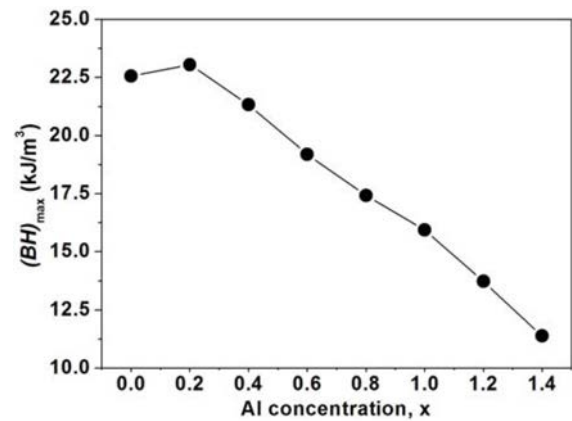


Fig. 7. The maximum energy product $[(BH)_{\max}]$ as a function of Al concentration (x) for the M-type hexaferrite $\text{Sr}_{0.1}\text{Ca}_{0.6}\text{La}_{0.3}\text{Al}_x\text{Fe}_{12-x}\text{O}_{19}$ magnets.

This should be the reason for the variation of H_{cb} with Al concentration (x).

Fig. 7 shows the influence of Al concentration (x) on the maximum energy product $[(BH)_{\max}]$ of the M-type hexaferrite $\text{Sr}_{0.1}\text{Ca}_{0.6}\text{La}_{0.3}\text{Al}_x\text{Fe}_{12-x}\text{O}_{19}$ magnets. It is clear that $(BH)_{\max}$ first increases with Al concentration (x) from 0.0 to 0.2, and then decreases when Al concentration (x) ≥ 0.2 . The maximum energy product of the M-type hexaferrite magnets is estimated by the product between the coercivity field and remanent magnetization, and is considered as a comparative indication of the hysteresis area.

Conclusions

The ceramic process was used to prepare the Al substituted M-type hexaferrites $\text{Sr}_{0.1}\text{Ca}_{0.6}\text{La}_{0.3}\text{Al}_x\text{Fe}_{12-x}\text{O}_{19}$ ($0 \leq x \leq 1.4$). The XRD patterns of the magnetic powders at Al content (x) ≤ 0.8 show the M-type strontium hexaferrite phase with $\alpha\text{-Fe}_2\text{O}_3$ as a second phase. At Al content (x) ≥ 1.0 , there are single magnetoplumbite phase patterns. The images of the M-type hexaferrite magnets show that the grain particles of the magnets are hexagonal platelet-like shape, and the grain size decreases with the increase of Al concentration (x). B_r decreases with Al content (x) from 0 to 1.4. The H_{cj} increases with Al content (x) from 0 to 1.4. While H_{cb} first increases with Al content (x) from 0 to 0.6 and then decreases at Al content (x) ≥ 0.6 . $(BH)_{\max}$ first increases with Al concentration (x) from 0.0 to 0.2, and then decreases at Al concentration (x) ≥ 0.2 .

Acknowledgements

This work was supported by National Natural Science Foundation of China (No. 51272003 and No. 51472004), Scientific Research Fund of Sichuan Provincial Education Department (No. 13ZA0918, No. 14ZA0267 and No.

16ZA0330), the Major Project of Yibin City of China (No. 2012SF034 and No. 2016GY025), Scientific Research Key Project of Yibin University (No. 2015QD13) and the Open Research Fund of Computational Physics Key Laboratory of Sichuan Province, Yibin University (No. JSWL2015KFZ04).

References

1. J. Dho, E.K. Lee, J.Y. Park, N.H. Hur, *J. Magn. Magn. Mater.* 285 (2005) 164-168.
2. A. Mali, A. Ataie, *Scri. Mater.* 53 (2005) 1065-1070.
3. Y.Q. Li, Y. Huang, S.H. Qi, F.F. Niu, L. Niu, *J. Magn. Magn. Mater.* 323 (2011) 2224-2232.
4. W. Abbas, I. Ahmad, M. Kanwal, G. Murtaza, I. Ali, M.A. Khan, M.N. Akhtar, M. Ahmad, *J. Magn. Magn. Mater.* 374 (2015) 187-191.
5. B.H. Bhat, B. Want, *Appl. Phys. A*, 122 (2016) 148-155.
6. I. Ahmad, M. Ahmad, I. Ali, M. Kanwal, M.S. Awan, G. Mustafa, M. Ahmad, *J. Electron. Mater.* 374 (2015) 187-191.
7. A. Awadallah, S.H. Mahmood, Y. Maswadeh, I. Bsoul, M. Awawdeh, Q.I. Mohaidat, H. Juwhari, *Mater. Res. Bull.* 74 (2016) 192-201.
8. D.A. Vinnik, A.S. Semisalova, L.S. Mashkovtseva, A.K. Yakushechkina, S. Nemrava, S.A. Gudkova, D.A. Zhrebtssov, N.S. Perov, L.I. Isaenko, R. Niewa, *Mater. Chem. Phys.* 163 (2015) 416-420.
9. R. Ezhil Vizhi, V. Harikrishnan, P. Saravanan, D. Rajan Bahu, *J. Cryst. Growth* 452 (2016) 117-114.
10. S.V. Trukhanov, A.V. Trukhanov, V.G. Kostishin, L.V. Panina, I.S. Kazakevich, V.A. Turchenko, V.V. Oleinik, E.S. Yakovenko, L. Yu. Matsui, *J. Exp. Theor. Phys.* 123 (2016) 461-469.
11. Y.J. Yang, F.H. Wang, J.X. Shao, X.S. Liu, D.H. Huang, *J. Ceram. Soc. Japan* 125 (2017) 27-31.
12. S. Jauhar, J. Singh, K. Chandra, S. Bansal, S. Singhal, *Powder. Technol.* 212 (2011) 193-197.
13. P. Sharma, R.A. Rocha, S.N. de Medeiros, A. Paesano Jr, B. Hallouche, *Hyperfine Interact.* 175 (2004) 77-84.
14. H.Z. Wang, B. Yao, Y. Xu, Q. He, G.H. Wen, S.W. Lang, J. Fan, G.D. Li, L. Shan, B. Liu, *J. Alloys Compd.* 537 (2012) 43-49.
15. A.H. Najafabadi, R. Mozaffarinia, A. Ghasemi, *J. Supercond. Nov. Magn.* 28 (2015) 2821-2830.
16. Y.J. Yang, X.S. Liu, D.L. Jin, Y.Q. Ma, *Mater. Res. Bull.* 59 (2014) 37-41.
17. X.Q. Shen, M.Q. Liu, F.Z. Song, *Appl. Phys. A* 104 (2011) 109-116.
18. Y.J. Yang, X.S. Liu, *Mater. Tech.* 29 (2014) 232-236.
19. M.J. Iqbal, S. Farooq, *J. Alloys Compd.* 505 (2010) 560-567.
20. H.M. Khan, M.U. Islam, Y.B. Xu, M.A. Iqbal, I. Ali, *J. Alloys Compd.* 589 (2014) 258-262.
21. Z.Y. Chen, F. Wang, S.Q. Yan, Z.K. Feng, *Mater. Sci. Eng. B* 182 (2014) 69-73.
22. Y.J. Yang, F.H. Wang, J.X. Shao, X.S. Liu, S.J. Feng, J.S. Yang, *J. Magn. Magn. Mater.* 401 (2016) 1039-1045.
23. X. Li, W.G. Yang, D.X. Bao, X.D. Meng, B.Y. Lou, *J. Magn. Magn. Mater.* 329 (2013) 1-5.
24. Y.J. Yang, F.H. Wang, J.X. Shao, D.H. Huang, X.S. Liu, S.J. Feng, C.E. Wen, *J. Magn. Magn. Mater.* 384 (2015) 64-69.
25. Z.F. Zi, Y.P. Sun, X.B. Zhu, Z.R. Yang, J.M. Dai, W.H. Song, *J. Magn. Magn. Mater.* 320 (2008) 2746-2751.
26. D.H. Choi, S.Y. An, S.W. Lee, I.-B. Shim, C.S. Kim, *Phys. Stat. Sol. (b)*, 241 (2004) 1736-1739.
27. J.X. Qiu, Q.G. Zhang, M.Y. Gu, H.G. Shen, *J. Appl. Phys.* 98 (2005) 103905.
28. Y.J. Yang, F.H. Wang, X.S. Liu, J.X. Shao, S.J. Feng, D.H. Huang, M.L. Li, *J. Magn. Magn. Mater.* 422 (2017) 209-215.
29. Z.M. Wang, *Ferrite Production Technology*, Chongqing University Press, Chongqing, 2013.